scientific reports

Check for updates

OPEN

A novel, low-cost clay ceramic membrane for the separation of oil-water emulsions

Dema Almasri[1,2]✉, Yehia Manawi[2]✉, Suhde Makki[3], Nafia Tasneem[3], Simjo Simson[2], Iman Abdel-Hadi[4], John Agcaoili[5], Jenny Lawler[2] & Viktor Kochkodan[2]✉

The development of a facile and efficient method for the fabrication of ceramic membranes fills a vital gap in the ceramic membrane manufacture research field. Ceramic membranes are relatively high in cost due to the cost of raw materials (metal oxides) as well as the energy required during the sintering stage of the fabrication process. In this study, a ceramic membrane made of low-cost halloysite nanotubular (HNT) clay is fabricated through a die press process and sintered at temperatures notably lower than those required of raw materials in commercial membranes. The features of the membrane were evaluated in terms of chemical properties, surface characteristics, hydrophilicity, durability, oil rejection performance, and antifouling properties. The pore size, porosity, and water permeability corresponding to the optimum membrane composition: halloysite: Al_2O_3: starch as 60:25:15 wt% were found to be 230 nm, 62.4%, and 1040 LMH/bar, respectively. The membrane demonstrated to be superhydrophilic in air and superoleophobic underwater. The performance tests were conducted with oil emulsions. Oil-water rejection tests were conducted at different concentrations of oil-in-water emulsions (724 and 1014 mg/L) and oil rejection was observed to reach more than 99%. The flux recovery ratio (FRR) of the membrane in the first filtration cycle when treating the lower oil concentration emulsion was 54% greater than the FRR corresponding to the higher oil concentration emulsion. However, in the next filtration cycle, the FRR of the ceramic membrane was 30% greater for the higher oil concentration emulsion which could be attributed to the formation of an oil film, preventing further oil particle penetration in the membrane matrix. The testing with real produced water from gas extraction indicated that the novel HNTs-based ceramic membrane performed well in feed solutions with high total dissolved solids content and can be used for produced water pretreatment before reverse osmosis membranes if the produced water to be desalted. The results from this work show that the developed ceramic membrane could be a promising, low-cost alternative to the ones existing in the current market for oily wastewater treatment.

Keywords Ceramic membrane, Filtration, Oily wastewater treatment, Membrane fouling

It is unquestionable that the treatment of oily wastewater is a necessity for our current time, especially with the increased demand of oil and gas, an industry which produces about 25.5 billion bbl. per year of produced water in the United States alone[1]. Environmental regulations related to the discharge of oily wastewater have become more stringent throughout the years, where country-specific limits for maximum oil concentrations typically lie in the range of 5 to 40 mg/L[2]. These large quantities of oily wastewater cause a substantial motivation to search for treatment approaches that utilize advanced materials and technologies.

Conventional oily wastewater treatment methods include dissolved air flotation, coagulation, flocculation, and biodegradation[3–6]. The choice of the most effective oil-water separation technology largely depends on the form of oil in water, i.e., free oil (> 150 μm), dispersed oil (20–150 μm), and emulsified oil (< 20 μm). Membrane technology is capable of separating oil droplets smaller than 10 μm, depending on the membrane pore size[7].

The oil may be separated from wastewater by ultrafiltration (UF), microfiltration (MF), or nanofiltration (NF) processes depending on the characteristics of the oil-water emulsion[8]. Currently, polymeric membranes

[1]Earthna-Center for a Sustainable Future, Qatar Foundation, P.O. Box 5825, Doha, Qatar. [2]Qatar Environment and Energy Research Institute, Hamad Bin Khalifa University, P.O. Box 34110, Doha, Qatar. [3]Chemical Engineering Program, Texas A&M University at Qatar, Education City, 23874 Doha, Qatar. [4]Division of Sustainable Development, College of Science and Engineering, Hamad Bin Khalifa University, Qatar Foundation, Doha, Qatar. [5]HBKU Core Labs, Hamad Bin Khalifa University, Qatar Foundation, PO Box 34110, Doha, Qatar. ✉email: delmasri@hbku.edu.qa; ymanawi@hbku.edu.qa; vkochkodan@hbku.edu.qa

dominate the commercial membrane market[9]. This is due to well established fabrication techniques and the relatively low-cost of large-scale production of polymer membranes. While polymeric membranes have these advantages, they are sensitive to harsh feedwater conditions, are not resistant towards different organic solvents, and their non-biodegradable nature is a concern in terms of long-term environmental pollution. Relative to polymeric membranes, ceramic membranes exhibit higher mechanical strength, are thermally and chemically more stable, are resistant to microbial degradation, are easy to regenerate, and usually have longer lifetime[10].

Although promising, the main obstacles in ceramic membrane practical applications are high membrane fabrication cost and membranes fouling. Colle et al.[11] tested an alumina ceramic membrane in an oil-in-water emulsion and observed nearly 84% reduction in flux after 40 min of process time due to fouling. Ebrahimi et al.[10] experimented with multilayer Al_2O_3 and TiO_2 ceramic membranes in oil-in-water emulsion and noticed about 70% reduction in flux after 60 min due to membrane fouling. Dong et al.[12] tested the performance of fabricated hollow fiber whisker-structured mullite-based ceramic membranes in a 1000 mg/L oil feed concentration and reported more than 84% reduction in flux within the first 60 min of operation. It is worth noting that ceramic membranes experience less irreversible fouling compared to their polymeric equivalents due to their more hydrophilic nature and ability to withstand harsh cleaning procedures[13,14].

Commercially available ceramic membranes are typically made of alumina (Al_2O_3), zirconia (ZrO_2), titanium oxide (TiO_2), silicon oxide (SiO_2), and non-metallic oxide ceramic material such as silicon carbide (SiC)[15]. The major reason why ceramic membranes are less dominant in the membrane market relative to their polymeric counterparts is because of the costly precursor material, complex fabrication technique and manufacturing process in terms of molding and sintering[16]. Having said that, most of the available commercialized ceramic membranes are fabricated from alumina. This is owing to alumina's low cost (relative to other metal oxides) as well as its exceptional physiochemical properties, such as its stability in acidic and basic pH, and its hydrophilic nature[17,18]. However, the preparation of alumina ceramic membranes requires high sintering temperatures, reaching 1600 °C[19]. Energy consumption during the sintering process accounts for at least 60% of the overall membrane cost[20]. The high sintering temperature adds to the manufacturing cost of the material, significantly increasing the ceramic membrane price in the market. Similar to alumina, the sintering temperatures required for titania and SiC ceramic membrane fabrication can reach up to 1450 °C[21] and 2100 °C[22], respectively.

The cost of manufacturing and raw materials makes typical ceramic membranes for industrial use quite costly. For instance, costs range from \$500/m^2 to \$1000/m^2 for an α-alumina porous tubular ceramic membrane with average pore sizes ranging from 1000 to 6000 nm[23]. As such, the reduction of fabrication costs is highly desirable for wider practical applications of ceramic membranes. The average cost of the ceramic membranes made from kaolin with pore sizes ranging between 550 and 810 nm was estimated to be \$220/m^2 [24]. While fabrication of a low-cost flat ceramic membrane with an average pore size of 4000 nm using kaolin and natural clay as a raw material was estimated to be \$130/m^2 [24]. The use of clay-based materials to reduce the fabrication cost of ceramic membranes was reported in literature. For instance, Khalil et al.[25] utilized local clay to prepare porous flat sheet ceramic membranes using die press technique for the removal of lead from water. The membranes, which were incorporated with graphite and activated carbon and sintered at 1400 °C, showed a water flux of 214 LMH at 1 bar and lead retention of 94%.

Moreover, Rawat and Bulasara[26] prepared clay-based membranes from kaolin and fly ash for the removal of humic acid from water. The membranes were reported to have a pore size range of 0.73–2.3 µm and porosities of 25–45% with membranes showing lower pore sizes and higher porosities when increasing kaolin loadings. The optimum membrane, made of 50% kaolin and 25% fly ash, showed humic acid rejection of 98% and flux of 720 LMH at 1 bar.

In this study, halloysite nanotubular (HNT) clay was used for ceramic membrane preparation. HNT is a natural clay mineral with a tubular structure. It has gained much attention recently due to its environmentally friendly nature, cost-effectiveness, abundance, and non-toxic nature[27]. HNT is widely studied for its application in the biomedical field[28], as a reinforcement filler in polymers[29], in environmental remediation[27], and engineering applications that involve high temperatures such as in ceramics[30]. The chemical composition of HNT is very similar to kaolin clay. Both are dioctahedral 1:1-layer aluminosilicates with a similar chemical formula, $Al_2Si_2O_5(OH)_4$. One difference is, kaolin has a plate-like structure, whereas HNT has a tubular morphology. Because of this morphology, HNT has a higher water content which includes a monolayer of water separating the unit layers in HNT[31].

This study presents a novel ceramic membrane made mainly of HNT and some Al_2O_3 content. To the best of our knowledge, the preparation of HNTs-based ceramic membranes for wastewater treatment applications was not reported in literature. This type of membrane is intended to be lower in cost than other materials used in the available market due to the more cost-effective HNT as well as the lower sintering temperature requirement during the fabrication process.

Experimental

Materials

HNT was purchased from Merck and had a particle length ranging between 68 and 1520 nm and external diameter ranging between 20 and 150 nm[27]. Al_2O_3 (activated, acidic, Brockmann I) were purchased from Sigma Aldrich and has a particle size of 150 mesh (~89 µm). Corn starch (ARGO, USA) was purchased locally from Doha, Qatar. Cooking oil (Thali, Qatar), a mixture of palm oil (70%) and sunflower oil (30%)) was used for the oil rejection tests.

Membrane fabrication

A mixture of HNT clay, Al_2O_3, and starch was ball milled (using a Retsch PM 200, Germany) at a rate of 100 rpm for 4 h. Table 1 shows the weight loadings (%) corresponding to HNTs, alumina, and starch which

	Loading (wt%)		
Membrane	HNTs	Al_2O_3	Starch
M1	100	0	0
M2	0	100	0
M3	60	35	5
M4	60	30	10
M5	60	25	15
M6	60	20	20
M7	70	30	0

Table 1. Weight loadings (%) corresponding to HNTs, Al_2O_3 and starch used for Preparation of ceramic membrane.

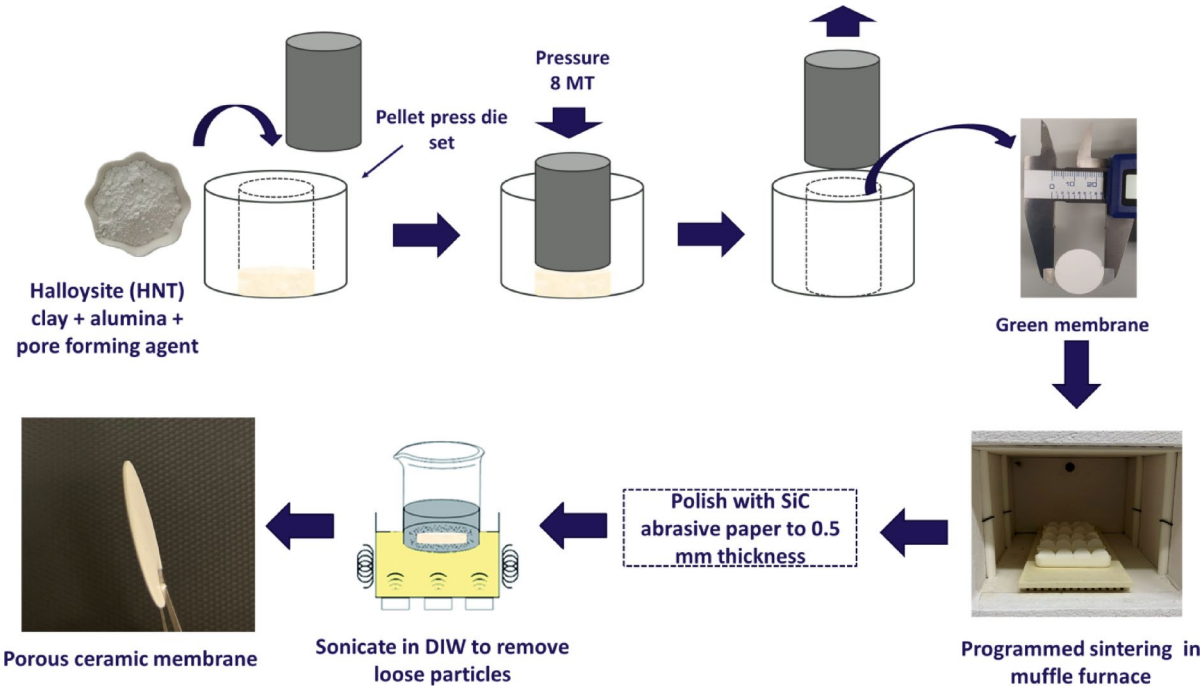

Fig. 1. Ceramic membrane fabrication process.

were investigated in the present work in order to identify the optimal composition for membrane fabrication. A schematic of the membrane fabrication process is shown in Fig. 1. The ball milled mixture was pressed in a 25 mm diameter die set by using a die press (Carver, Model 4389, USA). The sample was pressed at 8 metric tons for a period of 3.5 min. The ceramic discs were sintered to a temperature of 1100 °C using a muffle furnace (Nabertherm, Germany) with a 2 °C/min step size to prevent any cracks from forming due to phase changes. The sintered membranes were polished down to a thickness of 0.5 mm using a 320 grit, followed by a 600-grit abrasive paper.

Characterization of the HNTs based membrane

X-ray diffraction (XRD) analysis was conducted using a diffractometer (Rigaku Smartlab, Japan) equipped with a Cu Kα lamp (λ = 0.154 nm). An X-ray fluorescence (XRF) device (Rigaku ZSX Primus II Wavelength Dispersive, Japan) was used to perform elemental analysis. The surface and cross-section morphologies of the ceramic membranes were analyzed using a scanning electron microscope (SEM) (FEI Quanta 650 FEG, USA) at an accelerating voltage of 5 kV. Water contact angle measurements were performed using a contact angle analyzer (Krüss DSA25 Drop Shape Analyser, Germany). Dektak stylus profilometer (Bruker Corporation, Massachusetts, USA) was used to measure the average surface roughness (R_a) of the ceramic membranes in 3D mode with a scan speed of 66.67 µm/s. The profilometer scan area was 2000 µm × 2000 µm in which contact mode with the membrane surface using hills and valleys profile was implemented by recording the force received from the surface. Membrane microhardness was measured using a microhardness tester (Pace Technologies MHV-2000 Vickers, USA). The specific surface area of the ceramic membrane was measured with a BET surface area analyzer (Micromeritics ASAP 2420, USA) at 77 K. The thermogravimetric analysis (TGA) was carried out in order to monitor the reduction in sample's weight along with temperature. This will give an indication

about the nature and chemical composition of the analyzed samples. In the present paper, SDT Q600 TGA (TA instruments, Delaware, USA) was implemented under nitrogen environment starting from ambient temperature up to a temperature of 1480 °C with a heating rate of 10 °C/min.

Performance evaluation

Filtration tests

Membrane performance tests were conducted in a dead-end filtration cell (HP4750 stirred cell, Sterlitech, USA) with an effective filtration area of 5.29 cm^2. For the tests studying the effect of pressure on flux, the transmembrane pressure (TMP) varied from 0.5 to 7 bar. Unless otherwise stated, the filtration tests were conducted at a pressure of 1 bar at stirring speed of 800 rpm and performed in duplicates. The mass of the permeate was measured and the water flux J ($L/(m^2h)$) of the fabricated membrane was calculated using Eq. (1) and the water permeability L_p using Eq. (2):

$$J = \frac{V}{At} \tag{1}$$

$$L_p = \frac{J}{\Delta P} \tag{2}$$

where V denotes the volume of permeation (L), A indicates the effective surface area (m^2), P is the applied pressure in bar, and t denotes the filtration time in hours.

For the oil-rejection experiments, a solution comprised of 724 mg/L of oil was made using deionized water (DIW). Similarly, the fouling behavior of the ceramic membrane was evaluated by filtration using two solutions consisting of 724 mg/L (OW1) and 1014 mg/L (OW10) of oil were in DIW. The mixture was shaken at a rate of 400 rpm for at least 4 h and immediately used afterwards. All filtration experiments were conducted at room temperature under a constant pressure of 1 bar. Moreover, the oil-rejection filtration experiments were performed for 1 h while the fouling behavior experiments were conducted for 6 h. Permeate samples were taken at different filtration time intervals to measure the final total organic content (TOC) in mg/L. The rejection R (%) was calculated using Eq. 3:

$$R\,(\%) = \frac{C_f - C_p}{C_f} x100 \tag{3}$$

where C_f and C_p are the feed and permeate concentrations of oil, respectively.

The water absorption (%), density (g/cm^3), and porosity of the ceramic membranes were calculated using gravimetric methods[32,33] as follows:

$$Water\ Absorption\ (\%) = \frac{W_w - W_d}{A} \tag{4}$$

$$Density = \frac{\mathrm{W_d}}{\mathrm{V}} \tag{5}$$

$$\mathrm{Porosity}\ (\%) = \frac{\mathrm{W_w} - \mathrm{W_d}}{\mathrm{A}\,.\,l\,.\,\rho} \tag{6}$$

Where W_w and W_d denote the mass of the wet and dry membrane (g), A and V stand for the area and volume of the ceramic membrane (m^2), l denotes the thickness of the membrane (m), and ρ stands for the density of water at 25 ℃.

The pore sizes of the ceramic membranes were estimated using the Guerout–Elford–Ferry Eq. (7) [33]:

$$\mathrm{Pore\ size} = \sqrt{\frac{(2.9 - 1.75\,\epsilon\,)\,8\eta\,lQ}{\epsilon\,A\Delta\,P}} \tag{7}$$

Where ε is porosity, Q is the volume of permeate in m^3/s, η is the viscosity of water at 25℃ which equals 8.9×10^{-4} Pa s, and ΔP is the operational pressure, which is 1 bar.

Furthermore, the ceramic membranes were tested with real treated produced water collected from gas industry. The produced water had total dissolved solids (TDS) of 2358 mg/L, total organic carbon (TOC) of 981.9 mg/L and a pH 8.3. The effect of membrane washing on the performance of the ceramic membranes was evaluated by washing the fouled membranes with DIW (at pH 7) as well as with soap & water solutions (10 g/L) at pH 9.37 by placing the cleaning solutions in the filtration cell and stirring for 30 min at stirring speed of 800 rpm.

The flux recovery ratio (FRR) of the membranes was evaluated by filtration with DIW for 20 min followed by filtration with oil, sodium alginate or produced water and finally filtration with DIW again for 20 min. Equations (8–12) were used to estimate the total fouling ratio (R_{total}), reversible fouling ratio (R_r) as well as irreversible fouling ratio (R_{ir}) corresponding to the ceramic membranes[34,35]:

$$\mathrm{FRR} = \left(\frac{J_{DIW2}}{J_{DIW1}}\right) \tag{8}$$

$$R_{total}\,(\%) = \left(\frac{J_{DIW1} - J_{FS}}{J_{DIW1}}\right) \times 100 \tag{9}$$

$$R_{ir}\,(\%) = \left(\frac{J_{DIW1} - J_{DIW2}}{J_{DIW1}}\right) \times 100 \tag{10}$$

$$R_r = \frac{J_{DIW2} - J_{FS}}{J_{DIW1}} \times 100 \tag{11}$$

$$R_{total} = Ri + Rir \tag{12}$$

where J_{FS} stands for the flux collected with fouling solutions, J_{DIWA1} is the pure water flux and J_{DIWA2} is the pure water flux after filtration with fouling solutions. The experiments were repeated three times, and the average values were reported in this manuscript.

Analytical methods

The organic content of the feed and permeate streams was measured using a TOC analyzer (Shimadzu, Japan). TOC content was calculated by subtracting the total carbon (TC) from the inorganic carbon (IC) for each sample.

Results and discussion

Membrane characterization

Surface morphology, porosity, and permeability

SEM characterization of the membranes revealed the pure HNTs membrane (M1) to have a low porosity obviously due to the absence of the pore-forming agent (starch) which later showed to increase porosity within the membrane matrix. This can be confirmed by comparing the SEM cross section (Figure S1a) and top view of M1 (Figure S1b) relative to the other membranes. Similarly, M7 membrane, composed of 70 wt% HNTs and 30% alumina only had a dense membrane structure as shown in Figure S1e and Figure S1f.

On the other hand, the M2 membrane composed of pure alumina (Figure S1c and S1d) demonstrated a lack of robustness during the dry press formation and broke easily. Similarly, M3 membrane, composed of 60% HNTs, 35% alumina and 5% starch, depicted fragility and broke during the fabrication process.

Figures 2 and 3 depict the surface topography as well as the cross-section of M5 and M6 ceramic membranes. Compared to the pure ceramic membrane (M1), starch-containing ceramic membranes (M4, M5 and M6)

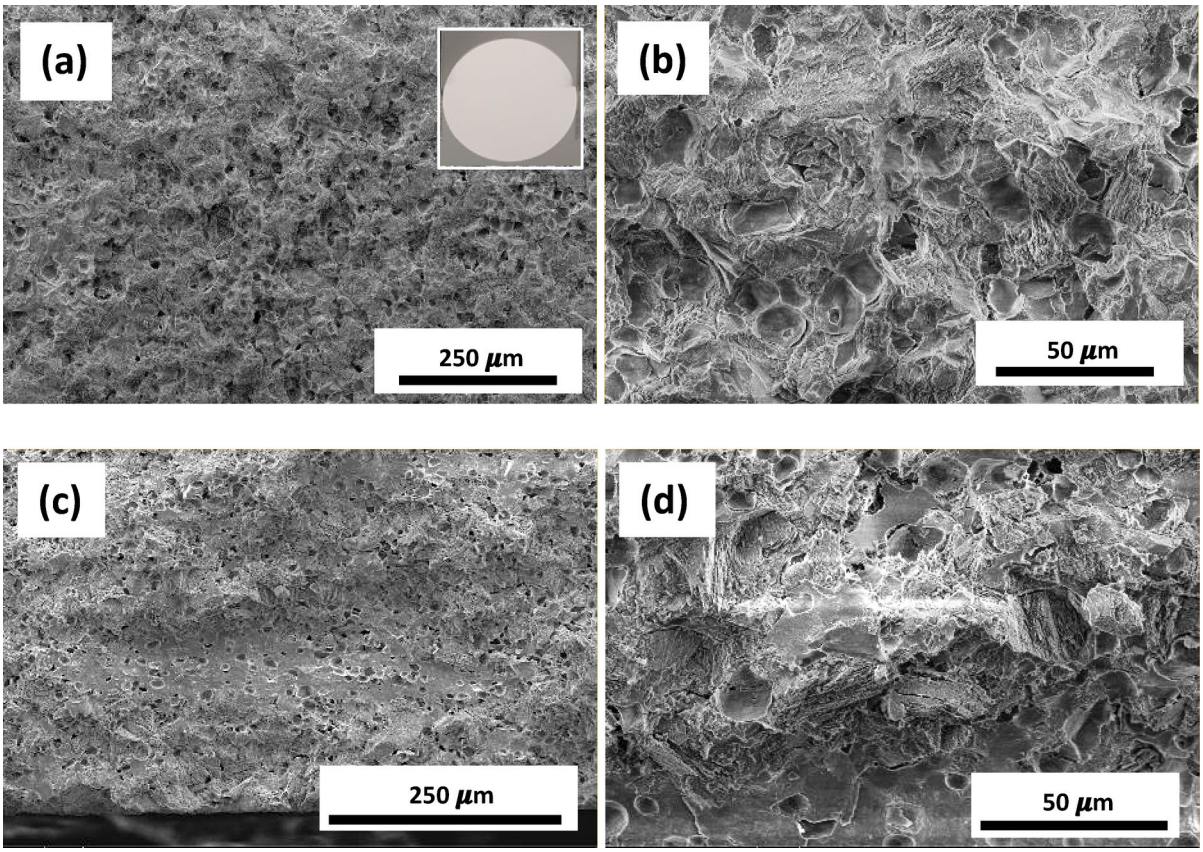

Fig. 2. SEM imaging of the surface topography (**a** & **b**) and cross section (**c** & **d**) of M5 membrane (inset: original ceramic membrane).

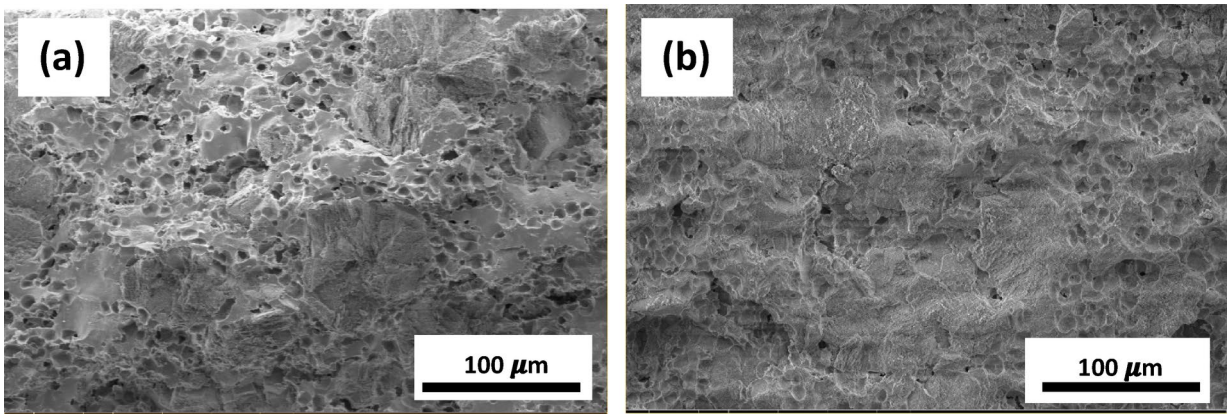

Fig. 3. SEM imaging of the cross section (**a**) and surface (**b**) topography of M6 ceramic membranes.

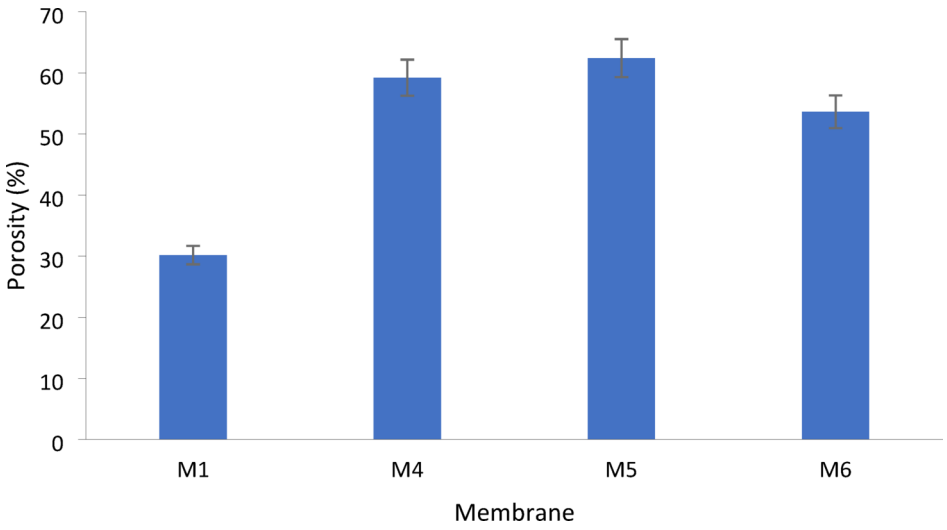

Fig. 4. Total porosity of fabricated ceramic membranes.

Membrane	Pore size (nm)	Density (g/cm^3)	Water absorption (%)
M4	46.85 ± 0.43	3.02 ± 0.0012	19.93 ± 0.24
M5	230.14 ± 3.69	2.56 ± 0.0114	24.34 ± 0.60
M6	308.86 ± 19.7	2.47 ± 0.0019	22.56 ± 1.93
M7	39.67 ± 0.83	3.40 ± 0.0019	16.29 ± 0.48

Table 2. Pore size, density and water absorption of ceramic membranes.

exhibited porous structures with visible differences in grain size due to the combination of HNTs clay and alumina. The pores observed on the surface were formed from the combustion of starch.

Based on the SEM analysis, most filtration experiments were conducted on ceramic membranes M4 to M6 as the membrane integrity was maintained.

The total porosity and permeate flux corresponding to the prepared membranes using DIW are depicted in Fig. 4. As seen, the addition of pore forming agent (starch) was observed to increase the porosity and flux of the developed ceramic membranes. This can be confirmed by comparing the porosities of M4, M5 and M6 with the pure HNTs membrane (M1). For instance, the average porosities of M4, M5 and M6 corresponded to 59,2, 62.4 and 53.6%, respectively while that of pure HNTs membrane was only 30.2%. This can be supported by observing the surface topography and cross section of the fabricated membranes using SEM (Fig. 2).

Table 2 shows the pore size, density and water absorption of the developed ceramic membranes. The addition of 10 wt% starch was observed to increase the pore size of pure membrane (M7) from 39.67 nm to 46.85 nm

(corresponding to M4). Likewise, the addition of 15 wt% and 20 wt% starch to ceramic membranes enhanced their pore sizes up to 230.14 and 308.86 nm, respectively.

The enhancement in the porosities and pore size following the addition of starch during the membrane preparation observed in the present work were found to be consistent with work reported in literature. For instance, Samhari et al.[36] reported that adding corn starch (15 wt%) increased the porosity of ceramic membrane from 12.3 to 58.6% and pore size from 1900 to 3500 nm. The authors attributed the increase in the pore size of the membranes to take place throughout the sintering process. Furthermore, in a study by Elomari and coworkers[37], ceramic membrane prepared from clay showed increased pore size from 1900 to 2400 nm and porosity from 30.8 to 48.2% as the starch content increased from 0 to 20 wt%, respectively. The increase in the porosity was attributed to the combustion of starch compounds during the sintering process.

Table 2 shows the density (g/cm^3) and water absorption (%) values of the prepared ceramic membranes. As seen in this table, the addition of starch has the effect of reducing the membrane's density. For instance, the density of M7 corresponding to 70 wt% HNTs and 30 wt% alumina was 3.4 g/cm^3. The addition of 5 wt% starch to ceramic membranes was found to lower the density of M4 down to 3.02 g/cm^3. The further addition of starch reduced the density of M5 (10 wt% starch) and M6 (20 wt% starch) to 2.56 g/cm^3 and 2.47 g/cm^3, respectively. It was also observed that the increase in the starch content increased the water absorption of the prepared ceramic membranes from 16.29 to 22.56% (Table 2). Overall, the decrease in density and the increase in the water absorption of ceramic membranes with addition of starch was found to correlate well with the previously published studies The ceramic membranes developed by Li et al.[38] showed a drop in their densities from 1.3 g/cm^3 to 0.9 g/cm^3 following the addition of 30 wt% starch due to the formation of porous structure that increased the volume of voids within the starch-containing membranes. Likewise, the ceramic membrane fabricated by Samhari et al.[36] was reported to show increasing water absorption from 5.8 to 32.4% at 15 wt% starch content.

EDS and XRD analysis

The surface EDS-elemental mapping images of M5 shown in Fig. 5 confirm the uniform distribution of alumina particles within the membrane. Moreover, from the elemental quantification analysis conducted and presented in Fig. 5, the Si: Al ratio was measured to be approximately 1:2.

The ceramic membranes, fabricated and sintered at various temperatures (1000 °C to 1100 °C), were analyzed using XRD technique. The phase composition of the ceramic membranes at the different sintering temperatures was evaluated and is depicted in Fig. 6. At sintering temperatures between 1000 °C and 1100 °C, halloysite peaks do not appear as they become amorphous at high temperatures. However, quartz peaks are visible at all three sintering temperatures. The alumina content in different phases is the most prominently detected by XRD due to its high crystallinity. At lower temperatures of 1000 °C and 1050 °C, small alumina peaks are mainly observed for δ-Al_2O_3 and κ- Al_2O_3 phases. After 1000 °C, the θ-Al_2O_3 phase appears and is the dominant type at 1050 °C. At 1000 °C and 1050 °C, the α- Al_2O_3 phase (corundum) co-existed with the other alumina phases. However, the transformation of all the pure alumina to the stable α- Al_2O_3 with high crystallinity is observed at 1100 °C. These results are in good alignment with those in literature[39,40] which reported the existence of sharp peaks of α-Al_2O_3 starting from 1050 °C and the disappearance of all other alumina phases at a temperature above 1050 °C. The sharp peaks indicate relatively large grain sizes[39]. Corundum is known to have high mechanical and thermal stability[41].

Membrane hydrophilicity and surface roughness

The hydrophilicity of a membrane is one of the most crucial properties that affects its flux and fouling resistance. The contact angle of a water drop on the membrane surface indicates a membrane's hydrophilic/hydrophobic character[42]. A membrane with a superhydrophilic and superoleophobic character is necessary to effectively and efficiently reject oil while allowing water to pass through at a high flux[43]. The ceramic membrane, M5 is found to be superhydrophilic in air (water contact angle (WCA) = 0°) and superoleophobic under water (oil under-water contact angle (OCA) ≈ 172.9°) as depicted in Fig. 7. This can be attributed to numerous surface hydroxyl groups such as Si-OH and Al-OH as well as to the high surface roughness of the prepared membrane According to the Wenzel equation, a hydrophilic surface with a static contact angle, θ_0, less than 90° becomes more hydrophilic with the increase in the roughness factor[44,45]. Hence, due to the surface wetting properties, the prepared HNTs based membrane is expected to form an oleophobic layer of water molecules on the surface of the membrane that assists in repelling oil[12].

Membrane surface roughness plays an important role in the wettability and interaction between membranes and contaminants in water. The effect of surface roughness on membrane fouling has been a concept of debate by scientists for years[46–48]. For example, Lyu et al.[49] hypothesized that a high surface roughness would enhance the membrane's antifouling properties[49]. Figure 8 presents 3D scans of the surfaces of M4, M5 and M7 ceramic membranes using Dektak stylus profilometer while Table 3 lists the average surface roughness values (in μm) corresponding to these membranes. As seen, the introduction of starch was found to increase the pore size and porosity of the membranes which was reported to increase the surface roughness of the ceramic membrane. A study by Chou et al.[50] reported that roughness value was affected by the pore size when different coating layers were deposited on membrane support. The average surface roughness of M7, which is composed of 70 wt% HNTs and 30 wt% alumina, was 2006.44 ± 292 nm while that of M4 (containing 10 wt% starch) was 3630.15 ± 522 nm. Moreover, M5 which contains 15 wt% starch showed an average surface roughness of 3971.6 ± 543 nm which was higher than both M7 and M4. The surface roughness values of the ceramic membranes were observed to correlate with previous work in literature. For instance, the ceramic membrane support which was prepared by Zou et al.[20] from alumina and fly ash showed average surface roughness of 1471–2045 nm.

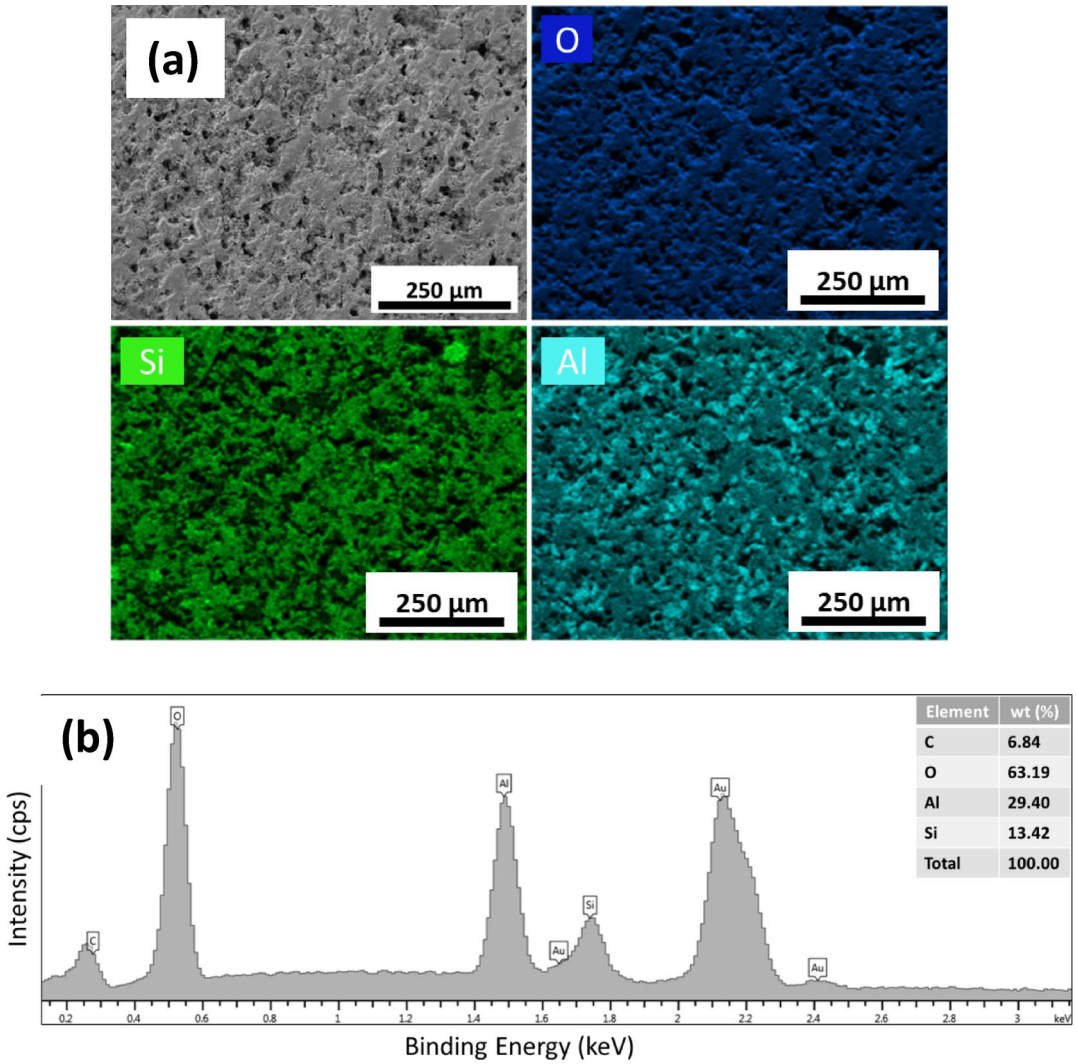

Fig. 5. (**a**) EDS elemental mapping of the ceramic membrane M5 surface and (**b**) EDS element quantification.

Zeta potential

The zeta potential of the pure alumina, HNTs particles as well as M5 ceramic membrane at different feed pH values is shown in Fig. 9. As seen, the zeta potential of pure alumina ranged between − 2.4 and − 34.5 mV while that of pure HNTs ranged between − 11.5 and − 39.5 mV. The zeta potential range of M5 ceramic membrane was found to range between − 13.1 to -36.2 mV. The increase in the negative surface charge of the modified membrane in comparison with pure alumina membrane could be attributed to the introduction of HNTs which were reported in literature to show negative surface charges over a wide range of pH[51,52]. Dong et al.[51] reported the zeta potential of HNTs to exhibit a negative surface charge starting from pH ~ 3 until a zeta potential of ~ -40 mV at pH 10. Moreover, Stor et al.[52] reported the existence of negative surface charges corresponding to HNTs over from pH 2.5 to pH 8. The increase in the negative surface charge of the ceramic membranes surfaces plays an important role on the interaction with fouling substances in water and, consequently, affect the antifouling properties of the membranes[53].

Mechanical properties

The microhardness or indentation hardness of a material is the measurement of the material's ability to withstand loads. Microhardness measurements were conducted on the membrane to determine the membrane response to stress. Figure 10a shows the microhardness of ceramic membranes using a microhardness tester. As seen, the addition of starch was found to reduce the hardness of the membranes due to the formation of a porous structure. For instance, M7 (composed of 70 wt% HNTs and 30 wt% alumina) depicted a microhardness of 133.9 HV while M4 (containing 60 wt% HNTs, 30 wt% alumina and 10 wt% starch) had a microhardness of 70.1 HV. The optimum membrane M5, which contains 60 wt% HNTs, 25 wt% alumina and 15 wt% starch, had a microhardness of 43.7 HV which was higher than a microhardness of 29 HV for M6 sample (60 wt% HNTs, 20 wt% alumina and 20 wt% starch(. Figure 10b depicts the indent which was formed after applying a force of 4.904 N on M5 which showed an average hardness of 43.71 HV. The findings of the present work were observed

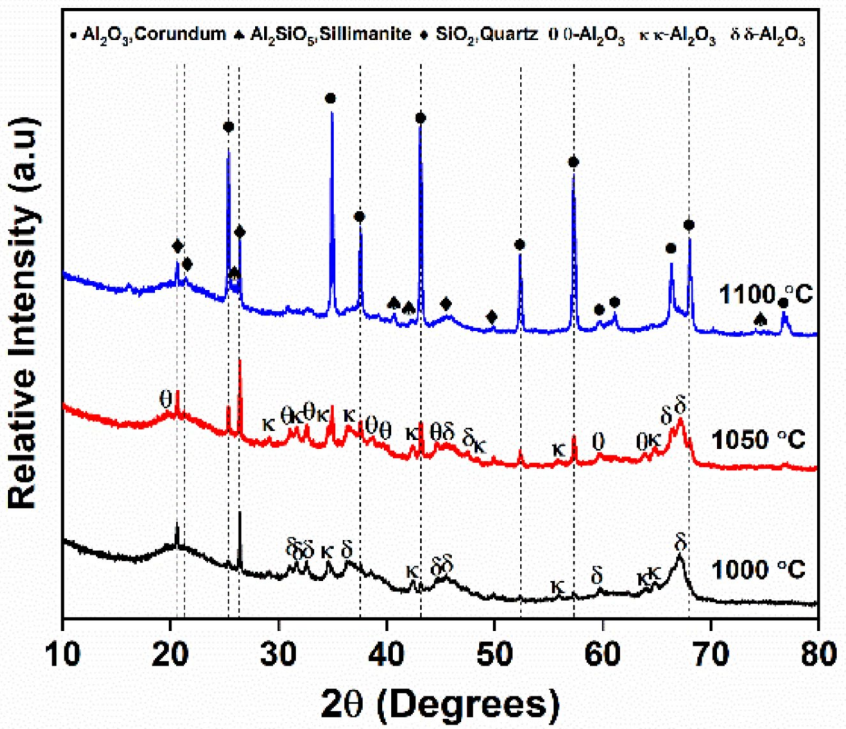

Fig. 6. XRD analysis with the phase compositions of the ceramic membrane M5 sintered at different temperatures.

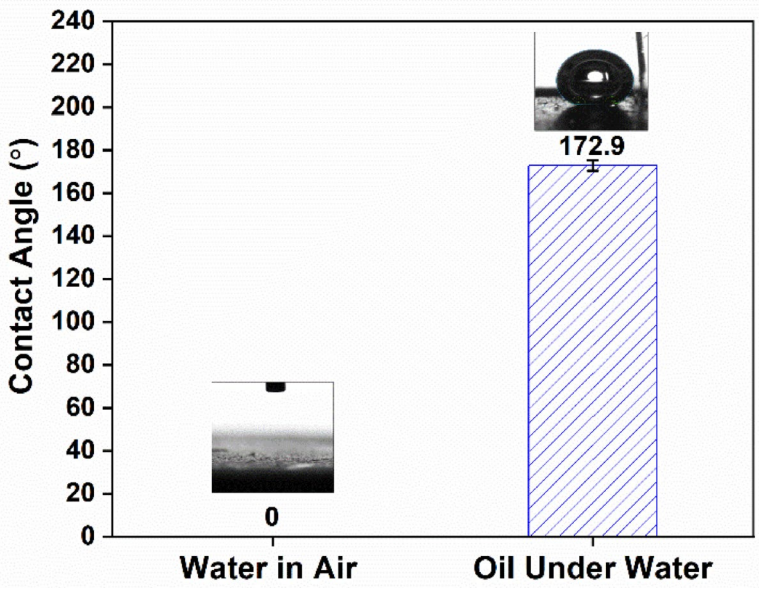

Fig. 7. Contact angle measurements of water in air (left) and oil underwater (right) of M5.

to be comparable with the work reported in literature. The measured microhardness of 43.71 in the present study falls within the microhardness range of 3D printed clay-based ceramic membranes sintered at 1300 °C andreported by Hwa and coworkers[54] which showed a microhardness range of 32–68 HV.

Thermogravimetric analysis (TGA)

TGA was conducted on ceramic membranes M5, M6 and M7 (Fig. 11). This test demonstrated that the addition of starch has an effect on the thermal behavior of the membranes. For instance, the first mass loss which occurred at around 80 °C is attributed to the evaporation of water in the ceramic membrane samples and is observed to be

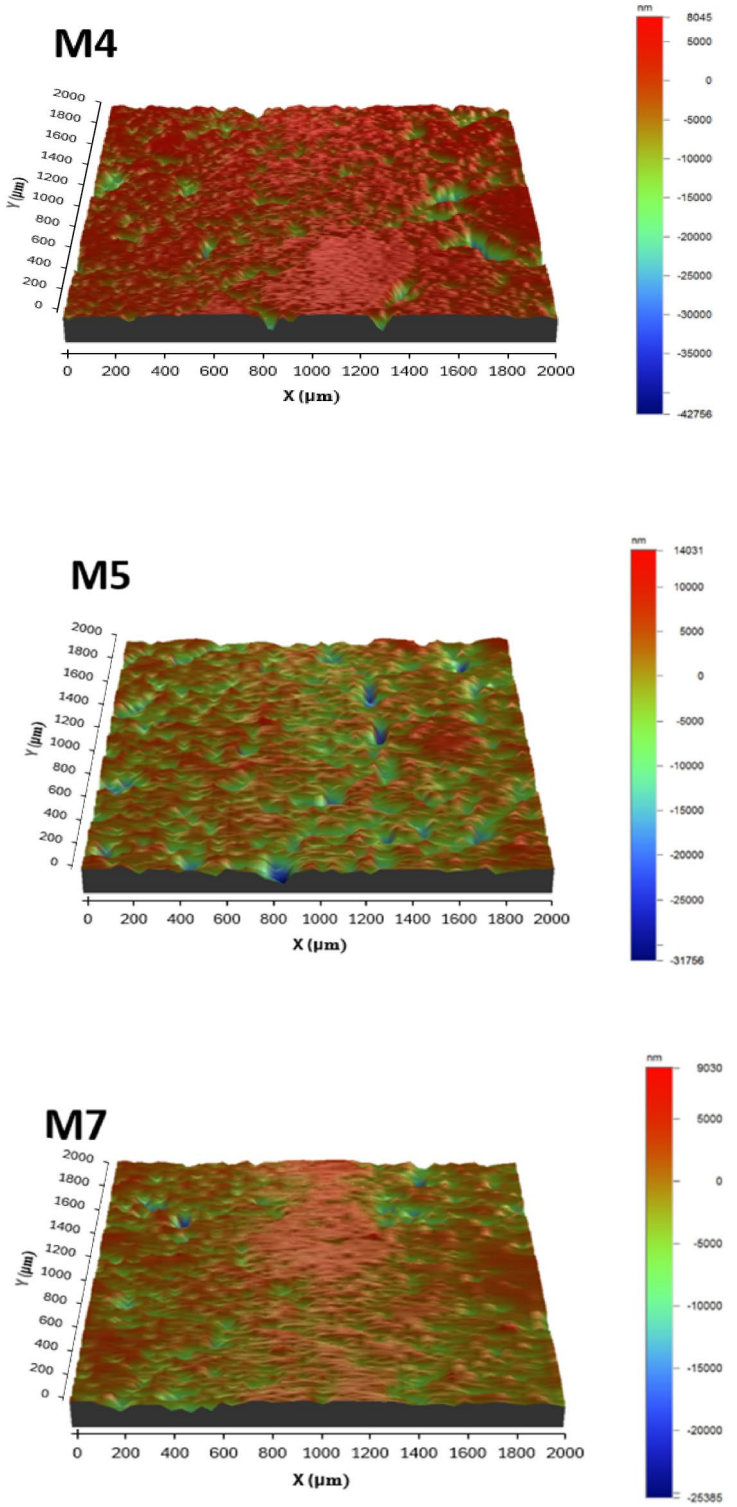

Fig. 8. surface roughness of ceramic membranes; M4: 60 wt% HNTs, 30 wt% alumina and 10 wt% starch. M5: 60 wt% HNTs, 25 wt% alumina and 15 wt% starch. M7: 70 wt% HNTs and 30 wt% alumina.

more pronounced in the sample containing 20 wt% starch compared to the sample with 15 wt% starch. This is due to the hydrophilic character of starch, which tends to absorb more water/moisture as a result of the presence of hydroxyl groups[55]. The second mass loss was observed to be initiated at approximately 300 °C due to the starch burning, and the membrane with 20 wt% starch loading exhibited a greater weight% loss when compared to the membrane with 15 wt% starch due to the higher starch content. This was observed to align with the TGA analysis performed by Guinesi et al.[56] and Dony et al.[57] who investigated the thermal behavior of starch under nitrogen and observed the thermal degradation to start around the temperature reported in the present work.

Membrane	Average surface roughness, (nm)
M4	3630.15 ± 522
M5	3971.6 ± 543
M7	2006.44 ± 292

Table 3. Average surface roughness of ceramic membranes.

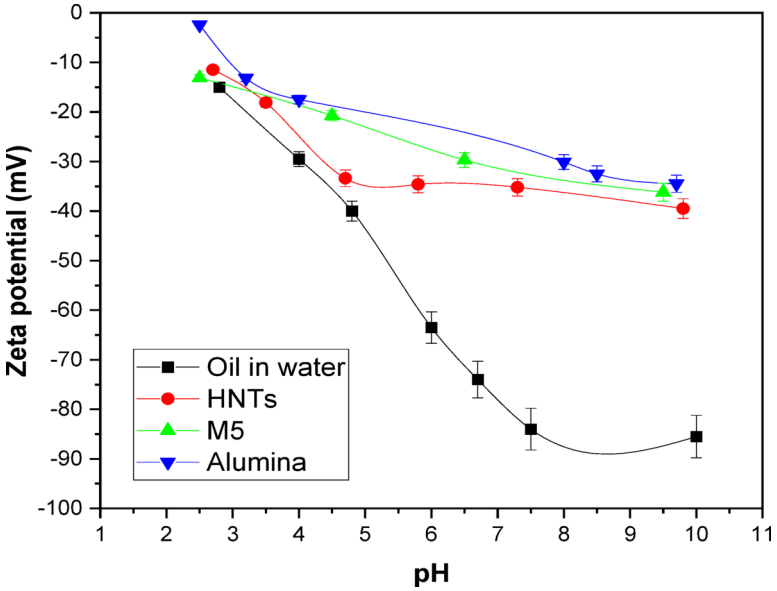

Fig. 9. Zeta potential of pure alumina, HNTs as well as M5 ceramic membrane at various pH.

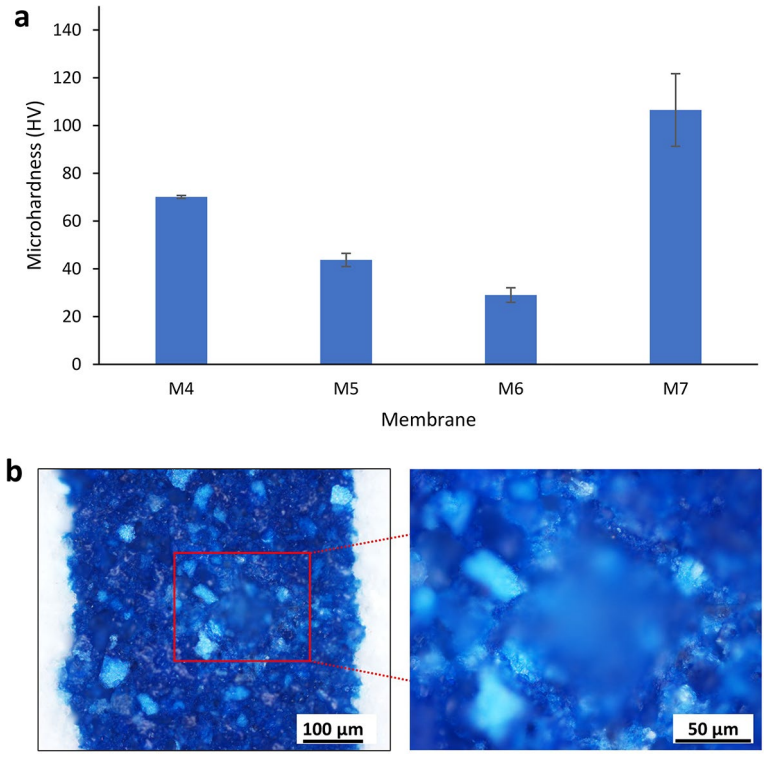

Fig. 10. (**a**) microhardness of ceramic membranes using microhardness tester and (**b**) indent formed after microhardness measurement test on M5 (Applied force = 4.904 N).

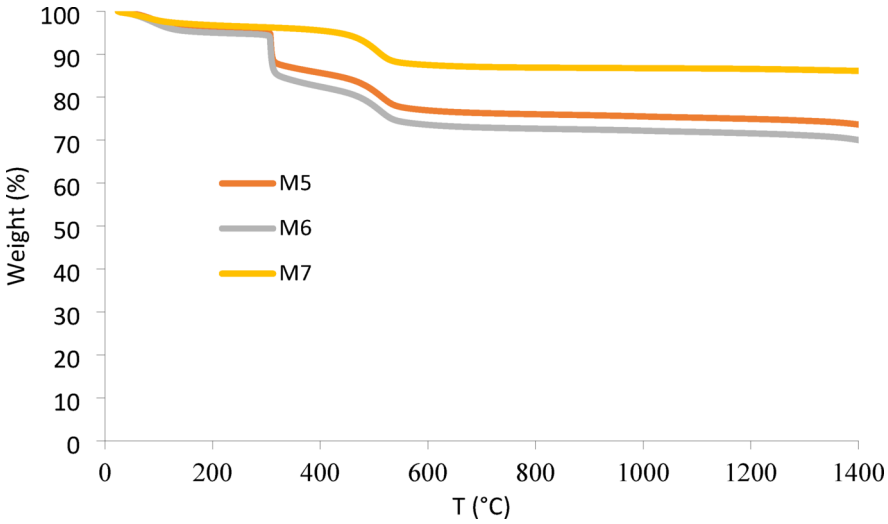

Fig. 11. TGA showing the thermal degradation of various loadings of ceramic membranes under nitrogen.

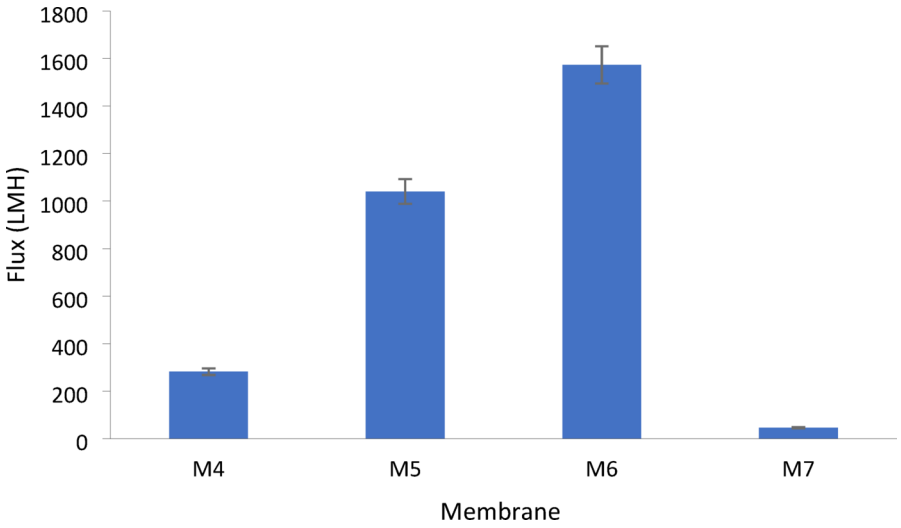

Fig. 12. Water fluxes of ceramic membranes during filtration with DIW; TMP: 1 bar.

The third mass loss shown in Fig. 11 took place at a temperature range of ~ 450 °C. This was attributed to the dehydroxylation process which was reported by Zhang et al.[58] to occur between 450 and 700 °C as shown in the below reaction. Above 700 °C, no visible mass loss was observed on the TGA curves under the studied temperature range.

$$Al2\,[Si2O5]\,(OH)4 \rightarrow\ Al2O3 \cdot 2SiO2\ +\ 2H2O$$

Membrane performance tests

Water fluxes of prepared membranes

Water fluxes for fabricated ceramic membranes are plotted in Fig. 12 and show an increase in flux values at higher starch content due to increase in the membrane porosity and pore size of the prepared membranes. In the present work, the enhancement in the pure water flux following the addition of starch was observed to outperform some of the work reported in literature. For comparison, Wu et al.[59], reported the permeability of a commercial tubular ultrafiltration membrane with a titania (TiO_2) support and a zirconia (ZrO_2) active layer to have a permeability of approximately 200 L/(m^2.hr.bar) with a molecular weight cut off (MWCO) of 150 kDa. Ben Ali and coworkers[60] reported a ceramic ultrafiltration membrane made of kaolino-illitic clay with a permeability of 2219 L/(m^2.hr.bar); however, it had a large median pore diameter of 6.3 µm. It should be mentioned that a fair comparison of the permeability of the ceramic membrane in this work with those presented by research is difficult to make due to the differences in pore size, porosity, and thickness of the studied membranes.

Membrane performance with oil emulsions

The rejection and flux of the prepared ceramic membranes during filtration experiments with oil emulsions is shown in Fig. 13a and b. It was observed that M5 sample exhibited the highest oil rejection with 99% removal efficiency during filtration of 1013 mg/L oily solutions compared with M4 and M6 membranes. Moreover, M4 sample exhibited a higher permeate flux of 60 ± 5 LMH relative to 41 ± 2.5 LMH for M5 membrane. The analysis of the correlation between starch loading and rejection showed that the addition of starch beyond 15% reduces the membrane rejection; hence, M5 with a starch loading of 15% was observed to correspond to the optimum ceramic membrane for oil rejection in the present work.

The increase in the oil rejection of membranes over filtration time can be attributed to formation of a compact layer composed of oil droplets on the membrane surface, which possess self-rejection properties towards oil. The confirmation of the presence of oil on top of the membrane was investigated using SEM and EDS elemental mapping techniques which are shown in Fig. 14a (surface of membrane before oil filtration) and Fig. 14b (surface of membrane after oil filtration). The EDS elemental maps which show an increase in the bright areas indicate a carbon mass content increase from 5.15% before oil filtration (Fig. 14c) to 11.15% after oil filtration (Fig. 14d).

Membrane fouling during filtration of oil emulsions

During filtration of oil emulsion, a decline in membrane permeate flux is usually observed. Permeate flux decline may occur due to internal and/or external pore blockage by oil in addition to the formation of a deposited oil layer on the surface of the membrane. Every one of these elements adds a level of resistance to the flow in the membrane, leading to flux decline. Figure 15a and b depict the membrane flux for the ceramic membrane during filtration of the oil emulsion with concentrations of 724 mg/L (OW1) and 1014 mg/L (OW10), respectively, in two consequent filtration cycles.

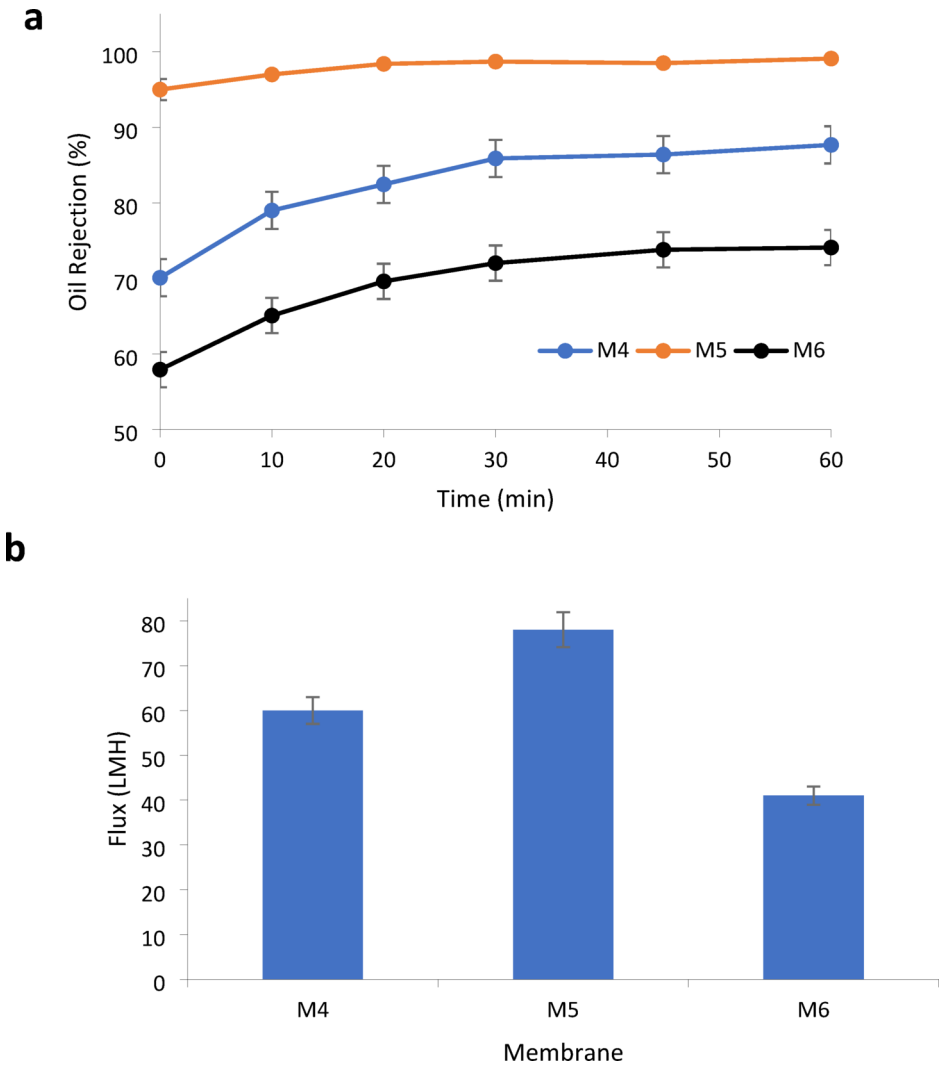

Fig. 13. (**a**) rejection and (**b**) flux of ceramic membranes by filtration of oily solutions (1013 mg/L); M4 (HNTs: 60 wt%, alumina:30 wt%, starch: 10 wt%), M5 (HNTs: 60 wt%, alumina: 25 wt%, starch: 15 wt%), M6 (HNTs: 60 wt%, alumina:20 wt%, starch: 20 wt%), TMP: 1 bar.

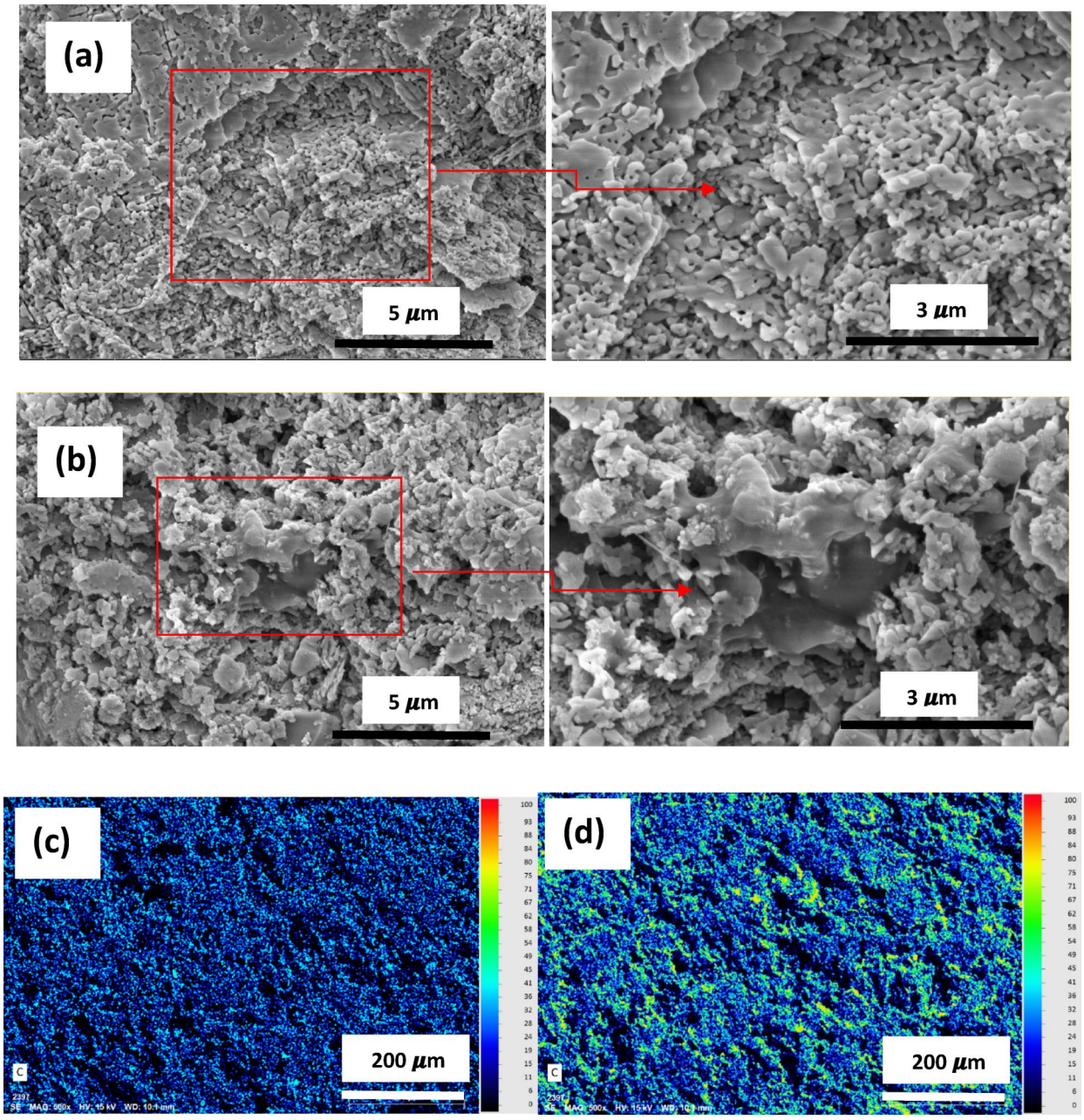

Fig. 14. SEM images and EDS elemental maps showing carbon at the top surface of M5 ceramic membrane before (**a**) and after (**b**) filtration with emulsified oil 1013 mg/L.

For the OW1 concentration, the permeate flux decreased significantly in the early stages in cycle 1. In cycle 2, nearly 84% of the permeate flux was regained. The permeate flux in cycle 2 decreased significantly initially but was steady within 4 h.

For the OW10 concentration, a gradual decrease of permeate flux in cycle 1 was observed and reached a steady state after 4 h. This indicates the occurrence of irreversible fouling in the membrane. The significant change in the permeate flux in cycle 2 was not major compared to that in cycle 1. This could be attributed to the formation of an oil layer on the membrane in cycle 2 which inhibited the mass transfer and consequential adsorption of small oil particles in the pores of the membrane. With time, more and more oil particles would cohesively bond together, including oil particles smaller than the membrane pore size, and water would pass though at a near steady flux.

The flux recovery ratio (FRR) is the measure of the ability of the membrane to recover its initial pure water flux after fouling to identify the extent of reversible and irreversible fouling occurring in the membrane. Figure 15c depicts FRR values. As OW1 emulsion is lower in oil concentration, a higher FRR (0.755) was observed relative to the FRR for the higher oil concentration OW10 for cycle 1 (0.344) as shown in Fig. 15c. However, after cycle 1,

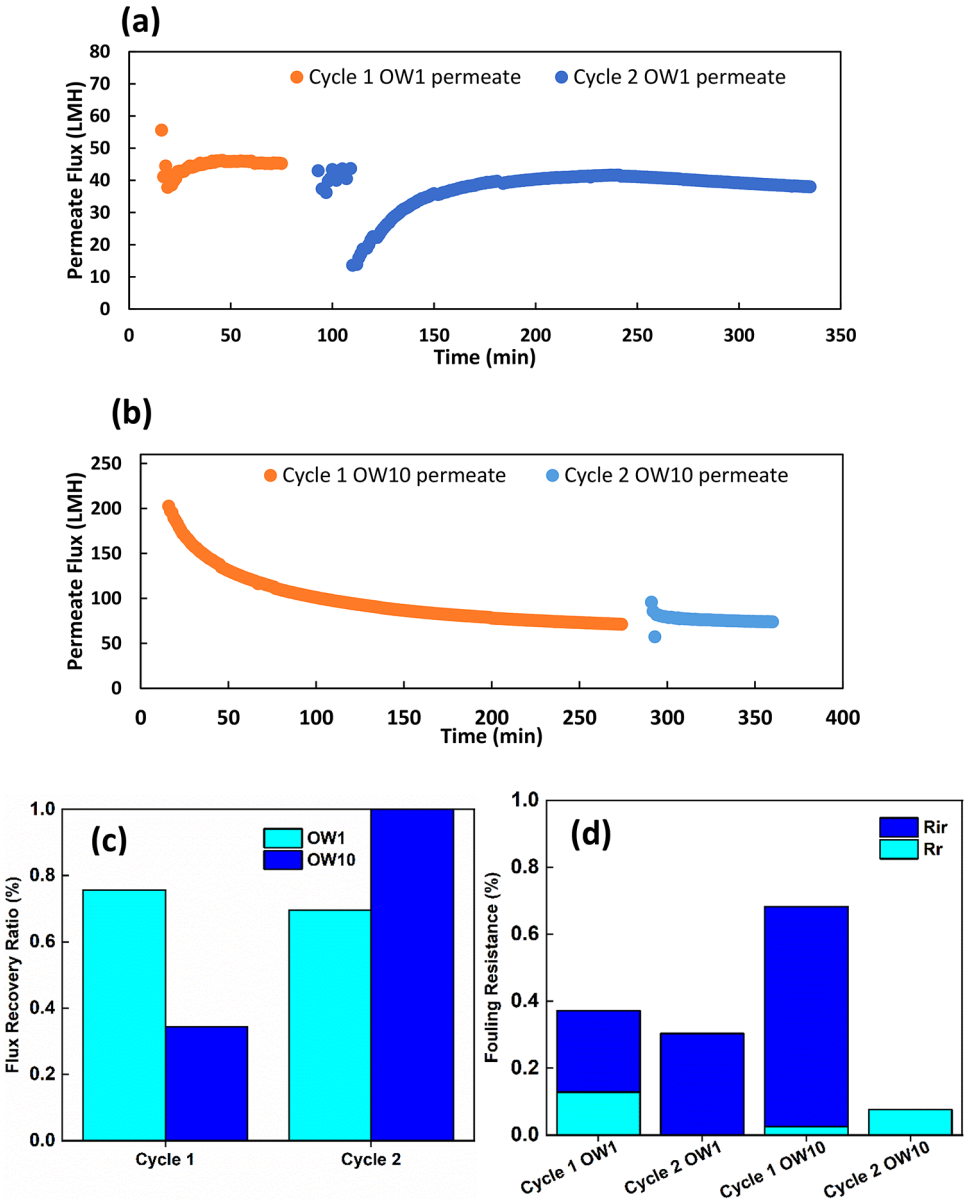

Fig. 15. (**a**) permeate flux of cycle 1 and cycle 2 for OW1 emulsion and (**b**) permeate flux of cycle 1 and cycle 2 for OW10 emulsion (**c**) Flux recovery ratio of the membrane with OW1 and OW2 emulsions for cycle 1 and cycle 2. (**d**) Fouling resistances of the membrane M5 during filtration of OW1 and OW2 emulsions for cycle 1 and cycle 2.

the larger particles of oil in OW10 remained on the surface and formed an oil layer, which may prevent further oil particles from passing through, hence, the FRR is higher for the OW10 in cycle 2 (0.999).

The reversible (R_r) and irreversible (R_{ir}) membrane fouling values are depicted in Fig. 15d. When looking at the fouling resistance of the membrane, OW1 consisted of smaller particles, hence, more oil particles could enter the membrane pore and be adsorbed internally, and more irreversible fouling in OW1 was observed throughout the overall performance of the membrane. In OW10, bigger oil particles allowed for more oil to be retained on the surface of the membrane which can be more easily removed via washing with water for cycle 2. The higher concentration of oil caused more irreversible fouling in the membrane in cycle 1 due to ultimate pore blocking; however, because the oil particles may have formed a layer on the external surface of the membrane in cycle 1, less membrane fouling is observed in cycle 2 as most of the oil is retained on the surface of the membrane. This indicates that physical cleaning with DIW could remove the loosely attached oil aggregates from the surface.

The noteworthy antifouling properties of the ceramic membranes could be attributed to the membrane's superoleophobicity as well as the membrane's overall negative surface charge as depicted in Fig. 9. The oil droplets in water are negatively charged and could be repelled from the negatively charged surface of M5 ceramic membrane thus notably reducing the membrane fouling during filtration. This was observed to align well with work reported in literature. For instance, the alumina ceramic membranes modified with SiC was reported

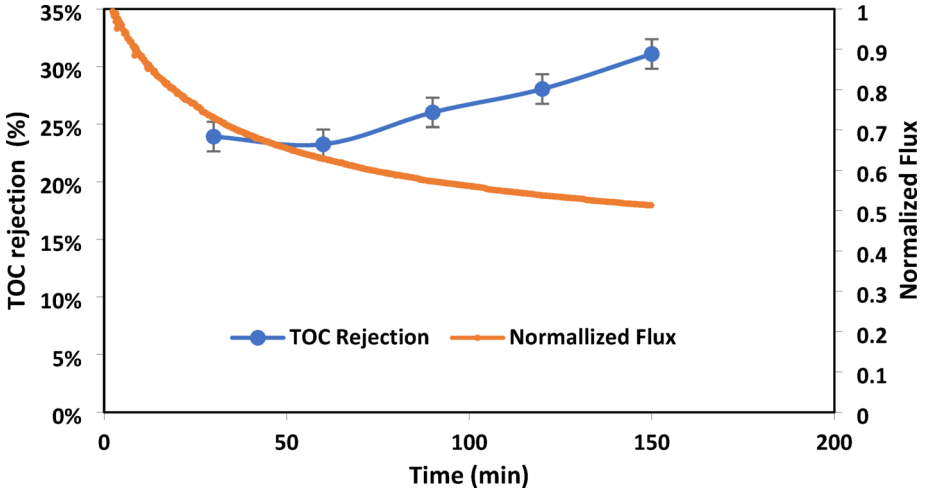

Fig. 16. TOC rejection and normalized flux corresponding to M5 during filtration of produced water; TMP: 2.5 bar, pH: 8.3.

by Chen et al.[61] to exhibit higher antifouling behavior when tested with oil/water solutions in comparison with pure alumina membranes due to changing in the modified membrane's surface charge from positive to negative and improvement of the membrane's hydrophilicity after modification with SiC. The investigation of the performance of the ceramic membranes modified by Chen et al.[61] during filtration with various concentrations of oil/water solutions showed that oil droplets exhibited characteristic negative surface charge ~ -70 mV and the repulsion between the modified membrane's surface and oil droplets in water enhance the antifouling properties of ceramic membranes.

It was reported that oil separation with MF and UF membranes is mainly dominated by size sieving mechanism and that membranes with smaller pore sizes have not only higher oil rejection but also possess lower irreversible fouling[62,63]. The membrane fouling in treatment of oily wastewater is largely affected by the membrane pore size. When the membrane pore size is smaller than oil droplets in water, the oil droplets can accumulate on the membrane surface which is followed by cake layer formation and pore blockage. The oil droplets can be forced to pass through the membrane at high operating pressures which results in lower oil fouling[64,65]. On the other hand, when the pore size of the ceramic membranes is greater than oil droplets in water the blockage of internal pores may take place and consequently, the selection of optimum pore size for treatment of oily wastewater with membranes is critical to reduce fouling[65].

Filtration of produced water

Ceramic membrane performance tests were further conducted using industrial produced water as feed to simulate practical application. The testing of the developed membranes was conducted by the filtration of real produced water from gas extraction in Qatar, which had a TDS of 2358 mg/L, TOC content of 981.9 mg/L and pH 8.3. Figure 16 shows the TOC rejection and normalized flux of M5 membrane during filtration of produced water. It can be observed that the normalized flux of M5 ceramic was above 51% at 150 min filtration time. Moreover, the effect of membrane washing on the performance of the ceramic membranes was evaluated as described in Sect. 2.4.1. It was found that FRR of ceramic membrane after cleaning with soap solutions was 21% which was significantly higher than that corresponding to washing with DIW (4%). The treatment of real produced water in the present work was observed to be in good agreement with work reported in literature. The commercial UF TiO_2/ZrO_2 composite membranes (TAMI Industries, France) were used to treat oil-sands process water with TOC 56.1 mg/L[66]. The commercial membranes showed similar TOC removal efficiencies of 24.8–38.6% despite having a lower TOC in the feed produced compared with feed produced water in the present work. The findings of this part indicate that the novel HNTs-based ceramic membrane can be used for produced water pretreatment before RO if water desalting is required as it performed well in high TDS feed solutions filtration.

Conclusions

Novel HNTs-based ceramic membranes were prepared by using a die press method and sintered at 1100 ℃, which is lower than the sintering temperature employed for fabrication of most of the commercial ceramic membranes. SEM surface topography images depicted a porous surface with a visible difference in grain size due to the combination of HNTs clay and alumina and alumina was found to be homogenously distributed throughout the membrane. Contact angle measurements revealed the membrane to be superhydrophilic and superoleophobic underwater. The pore size, porosity, and water permeability corresponding to the optimum membrane composition: halloysite: Al_2O_3: starch as 60:25:15 wt% were found to be 230 nm, 62.4%, and 1040 LMH/bar, respectively. The ceramic membrane showed a TOC rejection of 99.1% when tested with filtration of 1013 mg/L oil/water solutions. The FRR of the ceramic membrane in cycle 1 with OW1 and OW10 was 0.757 and 0.346, respectively, and 0.695 and 1.00 in cycle 2 for OW1 and OW2, respectively. When treating OW1,

irreversible fouling was observed in cycle 1 and cycle 2 of the oil emulsion treatment process, whereas irreversible fouling was observed only in cycle 1 with OW10 due to the larger oil particles present in OW10 which formed loosely attached oil aggregates on the membrane surface. Real produced water from gas extraction was used in the filtration tests and TOC rejection was observed to increase with time up to 33% while the normalized flux was 51% of the initial membrane flux. The findings of this study indicate that the prepared HNTs-based ceramic membrane can be used for efficient oil removal from oil/water emulsions as well as for produced water pretreatment before desalting RO membranes as they perform well in high TDS feed solutions. It should be highlighted that with the use of HNT clay, the cost of raw material and energy consumption for membrane fabrication can be notably reduced compared to conventional ceramic membranes available on the market.

Data availability

All data generated or analyzed during this study are included in this published article and its supplementary information files.

Received: 20 October 2024; Accepted: 17 April 2025
Published online: 25 April 2025

References

1. Consulting, A. U.S. Produced water volumes and management practices in 2021. 119 (2022).
2. Daud, N. M., Abdullah, S. R. S., Hasan, H. A. & Yaakob, Z. Production of biodiesel and its wastewater treatment technologies: a review. *Process Saf. Environ. Prot.* **94**, 487–508 (2015).
3. Zhao, C. et al. Application of coagulation/flocculation in oily wastewater treatment: A review. *Sci. Total Environ.* **765**, 142795. https://doi.org/10.1016/j.scitotenv.2020.142795 (2021).
4. Silva, F. et al. Dissolved air flotation combined to biosurfactants: a clean and efficient alternative to treat industrial oily water. *Reviews Environ. Sci. Bio/Technology*. **17** https://doi.org/10.1007/s11157-018-9477-y (2018).
5. Zhang, Z. The flocculation mechanism and treatment of oily wastewater by flocculation. *Water Sci. Technol.* **76**, 2630–2637. https://doi.org/10.2166/wst.2017.414 (2017).
6. Fadil, K., Chahlaoui, A., Ouahbi, A., Zaid, A. & Borja, R. Aerobic biodegradation and detoxification of wastewaters from the Olive oil industry. *Int. Biodeterior. Biodegrad.* **51**, 37–41. https://doi.org/10.1016/S0964-8305(02)00073-2 (2003).
7. Padaki, M. et al. Membrane technology enhancement in oil–water separation. A review. *Desalination* **357**, 197–207 (2015).
8. Song, Q., Qiu, L., Qiu, Q. & Cheng, R. in *6th International Conference on Energy and Environmental Protection (ICEEP 2017)*. 411–414 (Atlantis Press). (2017).
9. Yi, G., Fan, X., Quan, X., Chen, S. & Yu, H. Comparison of CNT-PVA membrane and commercial polymeric membranes in treatment of emulsified oily wastewater. *Front. Environ. Sci. Eng.* **13**, 1–9 (2019).
10. Ebrahimi, M. et al. Investigations on the use of different ceramic membranes for efficient oil-field produced water treatment. *Desalination* **250**, 991–996. https://doi.org/10.1016/j.desal.2009.09.088 (2010).
11. Del Colle, R., Fortulan, C. A. & Fontes, S. R. Manufacture of ceramic membranes for application in demulsification process for cross-flow microfiltration. *Desalination* **245**, 527–532 (2009).
12. Wu, H. et al. Treatment of oily wastewaters by highly porous whisker-constructed ceramic membranes: separation performance and fouling models. *Water Res.* **211**, 118042 (2022).
13. Liu, Z. et al. Distinction between polymeric and ceramic membrane in AnMBR treating municipal wastewater: in terms of irremovable fouling. *J. Membr. Sci.* **588**, 117229 (2019).
14. Xu, M. et al. Hydrophilic SiC Hollow fiber membranes for low fouling separation of oil-in-water emulsions with high flux. *RSC Adv.* **10**, 4832–4839 (2020).
15. Arumugham, T. et al. Recent developments in porous ceramic membranes for wastewater treatment and desalination: A review. *J. Environ. Manage.* **293**, 112925 (2021).
16. Dong, Y., Wu, H., Yang, F. & Gray, S. Cost and efficiency perspectives of ceramic membranes for water treatment. *Water Res.*, 118629 (2022).
17. Younssi, S. A., Breida, M. & Achiou, B. *Alumina membranes for desalination and Water treatment*InTech,. (2018).
18. Fung, Y. L. E. & Wang, H. Investigation of reinforcement of porous alumina by nickel aluminate spinel for its use as ceramic membrane. *J. Membr. Sci.* **444**, 252–258 (2013).
19. Wang, B. in *Encyclopedia of Membranes* (eds Enrico Drioli & Lidietta Giorno) 1–2Springer Berlin Heidelberg, (2015).
20. Zou, D. et al. One-step engineering of low-cost Kaolin/fly Ash ceramic membranes for efficient separation of oil-water emulsions. *J. Membr. Sci.* **621**, 118954 (2021).
21. Faber, M. K. J. H. H. Titania substrates and fabrication. France patent (1992).
22. Eray, E., Candelario, V. M. & Boffa, V. Ceramic processing of silicon carbide membranes with the aid of aluminum nitrate nonahydrate: preparation, characterization, and performance. *Membranes* **11**, 714 (2021).
23. Issaoui, M. & Limousy, L. Low-cost ceramic membranes: synthesis, classifications, and applications. *C. R. Chim.* **22**, 175–187 (2019).
24. Nandi, B., Uppaluri, R. & Purkait, M. Preparation and characterization of low cost ceramic membranes for micro-filtration applications. *Appl. Clay Sci.* **42**, 102–110 (2008).
25. Khalil, A. K. A. et al. Preparation and characterization of clay based ceramic porous membranes and their use for the removal of lead ions from synthetic wastewater with an insight into the removal mechanism. *Heliyon* **10**, e24939. https://doi.org/10.1016/j.heliyon.2024.e24939 (2024).
26. Rawat, M. & Bulasara, V. K. Synthesis and characterization of low-cost ceramic membranes from fly Ash and Kaolin for humic acid separation. *Korean J. Chem. Eng.* **35**, 725–733. https://doi.org/10.1007/s11814-017-0316-6 (2018).
27. Almasri, D. A., Saleh, N. B., Atieh, M. A., McKay, G. & Ahzi, S. Adsorption of phosphate on iron oxide doped Halloysite nanotubes. *Sci. Rep.* **9**, 1–13 (2019).
28. Shabeena, M. et al. Biocompatible pectin-functionalised-halloysite loaded Poly (vinyl alcohol) nanocomposite films for tissue engineering applications. *J. Drug Deliv. Sci. Technol.* **82**, 104320 (2023).
29. Zare, Y., Rhee, K. Y. & Park, S. J. A modified version of conventional Halpin-Tsai model for the tensile modulus of polymer Halloysite nanotube nanocomposites by filler network and nearby interphase. *Surf. Interfaces.* **36**, 102547 (2023).
30. Lampropoulou, P. & Papoulis, D. Halloysite in different ceramic products: A review. *Materials* **14**, 5501 (2021).
31. Lázaro, B. B. Halloysite and kaolinite: two clay minerals with geological and technological importance. *Revista De La. Acad. De Ciencias Exactas Físicas Químicas Y Naturales De Zaragoza*, 7–38 (2015).
32. Hieres Vettorazzi da SILVA. A. G. C. Physical-Mechanical Characterization Of Brazilian Natural Stones: Apparent Density, Porosity, Water Absorption, And Capillarity Determinations. 41, 769–778, (2022). https://doi.org/10.5016/geociencias.v41i03.16702

33. Yehia Manawi, V. K., Mahmoudi, E. & Johnson, D. J. Abdul Wahab Mohammad, Muataz Ali Atieh. Characterization and separation performance of a novel polyethersulfone membrane blended with Acacia gum. *Sci. Rep.* **15831** https://doi.org/10.1038/s41598-017-14735-9 (2017).
34. Manawi, Y., Kochkodan, V. & Mohammad, A. W. Ali Atieh, M. Arabic gum as a novel pore-forming and hydrophilic agent in polysulfone membranes. *J. Membr. Sci.* **529**, 95–104. https://doi.org/10.1016/j.memsci.2017.02.002 (2017).
35. Shen, X., Xie, T., Wang, J. & Wang, F. Improved fouling resistance of poly(vinylidene fluoride) membrane modified with poly(acryloyl morpholine)-based amphiphilic copolymer. *Colloid Polym. Sci.* **295**, 1211–1221. https://doi.org/10.1007/s00396-017-4117-6 (2017).
36. Samhari, O., Rabiller-Baudry, S. A. Y. M., Loulergue, P., Bouhria, M. & Achiou, B. Ouammou. Fabrication of flat ceramic microfiltration membrane from natural kaolinite for seawater pretreatment for desalination and wastewater clarification. *Desalin. Water Treat.* **194**, 59–68 (2020).
37. Elomari, H. et al. I. Elamrani. Influence of starch content on the properties of low cost microfiltration membranes. *J. Asian. Ceam. Soc.* **5**, 313–319 (2017).
38. Li, S. & Zhou, C. A. W. J. Effect of starch addition on microstructure and properties of highly porous alumina ceramics. *Ceram. Int.* **39**, 8833–8839. https://doi.org/10.1016/j.ceramint.2013.04.072 (2013).
39. Cava, S. et al. Structural characterization of phase transition of Al2O3 nanopowders obtained by polymeric precursor method. *Mater. Chem. Phys.* **103**, 394–399 (2007).
40. Kovarik, L., Bowden, M. & Szanyi, J. High temperature transition aluminas in δ-Al2O3/θ-Al2O3 stability range. *J. Catal.* **393**, 357–368 (2021).
41. Amrute, A. P., Jeske, K., Łodziana, Z., Prieto, G. & Schüth, F. Hydrothermal stability of High-Surface-Area α-Al2O3 and its use as a support for hydrothermally stable Fischer–Tropsch synthesis catalysts. *Chem. Mater.* **32**, 4369–4374 (2020).
42. Bouazizi, A. et al. Removal of dyes by a new nano–TiO2 ultrafiltration membrane deposited on low-cost support prepared from natural Moroccan bentonite. *Appl. Clay Sci.* **149**, 127–135 (2017).
43. Anis, S. F., Lalia, B. S., Hashaikeh, R. & Hilal, N. Hierarchical underwater oleophobic electro-ceramic/carbon nanostructure membranes for highly efficient oil-in-water separation. *Sep. Purif. Technol.* **275**, 119241 (2021).
44. Wenzel, R. N. Surface roughness and contact angle. *J. Phys. Chem.* **53**, 1466–1467 (1949).
45. Durán, I. R. & Laroche, G. Water drop-surface interactions as the basis for the design of anti-fogging surfaces: theory, practice, and applications trends. *Adv. Colloid Interface Sci.* **263**, 68–94 (2019).
46. Zhong, Z., Li, D., Zhang, B. & Xing, W. Membrane surface roughness characterization and its influence on ultrafine particle adhesion. *Sep. Purif. Technol.* **90**, 140–146 (2012).
47. Wang, M., Wang, J. & Jiang, J. Membrane fouling: microscopic insights into the effects of surface chemistry and roughness. *Adv. Theory Simulations.* **5**, 2100395 (2022).
48. Zhang, S. Surface roughness and membrane fouling. *Nat. Water.* **1**, 132–132 (2023).
49. Lyu, Z. et al. 3D-printed surface-patterned ceramic membrane with enhanced performance in crossflow filtration. *J. Membr. Sci.* **606**, 118138 (2020).
50. Chou, K. S., Kao, K. B., Huang, C. D. & Chen, C. Y. Coating and characterization of Titania membrane on porous ceramic supports. *J. Porous Mater.* **6**, 217–225. https://doi.org/10.1023/a:1009679929672 (1999).
51. Dong, C. et al. Novel self-healing anticorrosion coating based on L-valine and MBT-loaded Halloysite nanotubes. *J. Mater. Sci.* **53**, 7793–7808 (2018).
52. Stor, M., Czelej, K., Krasiński, A. & Gradoń, L. Exceptional sorption of heavy metals from natural water by Halloysite particles: A new prospect of highly efficient water remediation. *Nanomaterials* **13**, 1162 (2023).
53. Manawi, Y. et al. Characterization and separation performance of a novel polyethersulfone membrane blended with acacia gum. *Sci. Rep.* **7**, 15831 (2017).
54. Hwa, L. C. et al. Integration and fabrication of the cheap ceramic membrane through 3D printing technology. *Mater. Today Commun.* **15**, 134–142 (2018).
55. Shuzhen, N. et al. Enhancing hydrophobicity, strength and UV shielding capacity of starch film via novel co-cross-linking in neutral conditions. *Royal Soc. Open. Sci.* **5**, 181206 (2018).
56. Guinesi, L. S. et al. Kinetics of thermal degradation applied to starches from different botanical origins by non-isothermal procedures. *Thermochim. Acta.* **447**, 190–196. https://doi.org/10.1016/j.tca.2006.06.002 (2006).
57. Dony, P. & Thermogravimetric, F. B. Morphological and infrared analysis of blends involving thermoplastic starch and Poly (ethylene-co-methacrylic acid) and its ionomer form. *Molecules* **28**, 4519 (2023).
58. Xu, Z. B. et al. Thermal properties of Halloysite nanotubes (HNTs) intercalation complexes-A review. *E3S Web of Conferences* 131, (2019). https://doi.org/10.1051/e3sconf/201913101055
59. Barredo-Damas, S. et al. Ceramic membrane behavior in textile wastewater ultrafiltration. *Desalination* **250**, 623–628 (2010).
60. Ali, M. B., Hamdi, N., Rodriguez, M. A., Mahmoudi, K. & Srasra, E. Preparation and characterization of new ceramic membranes for ultrafiltration. *Ceram. Int.* **44**, 2328–2335 (2018).
61. Chen, M., Heijman, S. G., Luiten-Olieman, M. W. & Rietveld, L. C. Oil-in-water emulsion separation: fouling of alumina membranes with and without a silicon carbide deposition in constant flux filtration mode. *Water Res.* **216**, 118267 (2022).
62. Chen, M., Heijman, S. G. J. & Rietveld, L. C. Ceramic membrane filtration for oily wastewater treatment: basics, membrane fouling and fouling control. *Desalination* **583**, 117727. https://doi.org/10.1016/j.desal.2024.117727 (2024).
63. Ghidossi, R., Veyret, D., Scotto, J., Jalabert, T. & Moulin, P. Ferry oily wastewater treatment. *Sep. Purif. Technol.* **64**, 296–303 (2009).
64. Huang, A. et al. Fabrication of zinc oxide nanostructure coated membranes for efficient oil/water separation. *J. Membr. Sci.* **566**, 249–257 (2018).
65. Nagasawa, H., Omura, T., Asai, T., Kanezashi, M. & Tsuru, T. Filtration of surfactant-stabilized oil-in-water emulsions with porous ceramic membranes: effects of membrane pore size and surface charge on fouling behavior. *J. Membr. Sci.* **610**, 118210 (2020).
66. Alpatova, A. et al. Treatment of oil sands process-affected water with ceramic ultrafiltration membrane: effects of operating conditions on membrane performance. *Sep. Purif. Technol.* **122**, 170–182 (2014).

Acknowledgements

This work acknowledges and appreciates the use of the core laboratory facilities at the Qatar Environment and Energy Institute (QEERI) which include Dr. Said Mansour, Dr. Akshath Shetty, Dr. Ayman Samara, Dr. Atef Zekri, Mr. Janarthanan Ponraj and Mr. Mujaheed Pasha. The work also acknowledges MhdAmmar Hafiz. Their efforts and contribution are appreciated.

Author contributions

Dema Almasri: Conceptualization, Methodology, Investigation, Writing - Original Draft, Visualization. Yehia Manawi: Investigation, Writing - Review & Editing. Suhde Makki: Investigation, Writing-Original Draft. Nafia Tasneem: Investigation, Writing-Original Draft. Simjo Simson: Investigation. Iman Abdel-Hadi: Investigation. John Agcaoili: Investigation. Jenny Lawler: Writing - Review & Editing. Viktor Kochkodan: Validation, Writing

- Review & Editing.

Declarations

Competing interests
The authors declare no competing interests.

Additional information
Supplementary Information The online version contains supplementary material available at https://doi.org/10.1038/s41598-025-99143-0.

Correspondence and requests for materials should be addressed to D.A., Y.M. or V.K.

Reprints and permissions information is available at www.nature.com/reprints.

Publisher's note Springer Nature remains neutral with regard to jurisdictional claims in published maps and institutional affiliations.